

Accuracy of ghost-rotationally-invariant slave-boson and dynamical mean field theory as a function of the impurity-model bath size

Tsung-Han Lee¹, Nicola Lanatà², Gabriel Kotliar^{1,3}

¹*Physics and Astronomy Department, Rutgers University, Piscataway, New Jersey 08854, USA*

²*School of Physics and Astronomy, Rochester Institute of Technology,*

84 Lomb Memorial Drive, Rochester, New York 14623, USA and

³*Condensed Matter Physics and Materials Science Department,
Brookhaven National Laboratory, Upton, New York 11973, USA*

We compare the accuracy of the ghost-rotationally-invariant slave-boson (g-RISB) theory and dynamical mean-field theory (DMFT) on the single-band Hubbard model, as a function of the number of bath sites in the embedding impurity Hamiltonian. Our benchmark calculations confirm that the accuracy of g-RISB can be systematically improved by increasing the number of bath sites, similar to DMFT. With a few bath sites, we observe that g-RISB is systematically more accurate than DMFT for the ground-state observables. On the other hand, the relative accuracy of these methods is generally comparable for the quasiparticle weight and the spectral function. As expected, we observe that g-RISB satisfies the variational principle in infinite dimensions, as the total energy decreases monotonically towards the exact value as a function of the number of bath sites, suggesting that the g-RISB wavefunction may approach the exact ground state in infinite dimensions. Our results suggest that the g-RISB is a promising method for first principle simulations of strongly correlated matter, which can capture the behavior of both static and dynamical observables, at a relatively low computational cost.

I. INTRODUCTION

Quantum embedding approaches have recently attracted significant attention in condensed matter physics, material science, and quantum chemistry^{1–11}. The common idea of these approaches consists in mapping the original interacting lattice to an embedded quantum impurity model, whose parameters are determined self-consistently by matching the properties of the impurity model and the lattice. The dynamical mean-field theory (DMFT) is the first example of these approaches¹, which has become a standard method for strongly correlated materials². Nevertheless, the calculations of the dynamical Green's function in DMFT can be time-consuming for realistic multiorbital systems. Therefore, significant effort has been put into developing more efficient quantum embedding techniques^{4,5,8,12–15}.

The rotational-invariant slave-boson (RISB) mean-field theory and other related approaches are among the most efficient methodologies for studying strongly correlated systems^{4,7,8,13,14,16–20}. Unlike DMFT, these frameworks are often classified as static quantum embedding approaches, as the embedded impurity model parameters are determined self-consistently by matching the lattice and the impurity density matrix, instead of the local Green's function and self energy. These static quantum embedding approaches are particularly successful in capturing the static observables and low-energy spectral functions in strongly correlated systems in qualitative agreement with more sophisticated DMFT^{7,8,13}.

Recently, the ghost-RISB (g-RISB) extension has been introduced, where auxiliary ghost degrees of freedom are added to the non-interacting lattice model and the bath of the impurity model²¹. It has been shown that g-RISB with additional ghost orbitals can capture reliably

both the spectral and the static observables of the infinite dimensional Hubbard and Anderson lattice models^{21–25}. At the same time, a similar approach has been developed in the density matrix embedding theory^{26–28}, and the ancilla qubits technique²⁹.

The idea of increasing the bath size to improve the accuracy in g-RISB reminisces the bath discretization of dynamical mean-field theory with exact-diagonalization impurity solver (DMFT-ED)^{1,30,31}. In DMFT-ED, the continuous bath of the Anderson impurity model is fitted by a small number of bath orbitals such that the impurity model can be solved by ED. In the past decade, DMFT-ED has been extensively applied to the cluster extensions of DMFT and multiorbital realistic materials^{32–40}. Highly efficient exact-diagonalization techniques have also been developed^{41–46}.

Since the Hilbert space of the embedded impurity model grows exponentially with the number of the bath degrees of freedom in all the quantum embedding approaches, it is important to assess which method is more accurate and efficient at smaller bath sizes. Indeed, this is particularly important for frontier problems in strongly correlated materials or chemical systems, which generally involve multiple orbitals and/or large clusters^{32–40}. Nevertheless, the accuracy and the convergence behavior of g-RISB observables as a function of the bath size have not been systematically investigated yet.

In this work, we study the convergence behavior of g-RISB as a function of the number of bath orbitals in the single-band Hubbard model and compare it to DMFT-ED. Our results indicate that g-RISB generally provides us with more accurate energy and ground-state properties at small bath sizes, while the relative accuracy of these methods is comparable for the spectral properties. Moreover, we verify numerically that g-RISB satisfies the

variational principle in the limit of infinite coordination number, *i.e.*, that the energy decreases monotonically towards the exact value, suggesting that the g-RISB wavefunction may approach the exact ground state in infinite dimensions.

II. MODEL AND METHODS

We consider a single-orbital Hubbard model on the Bethe lattice in the limit of infinite coordination number¹:

$$H = \sum_{\mathbf{k}} \sum_{\sigma} \epsilon_{\mathbf{k}\sigma} c_{\mathbf{k}\sigma}^{\dagger} c_{\mathbf{k}\sigma} + \sum_i U n_{i,\uparrow} n_{i,\downarrow}, \quad (1)$$

where $c_{\mathbf{k}\sigma}^{\dagger}$ and $c_{\mathbf{k}\sigma}$ are the electron creation and annihilation operators for momentum \mathbf{k} and spin σ , $n_{i\sigma} = c_{i\sigma}^{\dagger} c_{i\sigma}$ is the number operator on site i , and U is the Coulomb interaction. The energy unit is set to $D = 1$, where D is the half bandwidth of the semicircular density of states on the Bethe lattice.

A. Ghost-rotationally-invariant slave-boson theory

The g-RISB approach is utilized to study the static observables and the dynamical spectral function of the single-orbital Hubbard model. The detailed derivations of g-RISB are shown in Refs. 21–23. Here, we briefly review the g-RISB formalism.

The g-RISB formalism is entirely encoded in the following Lagrangian²³:

$$\begin{aligned} \mathcal{L}[\Phi, E^c; R, \lambda; D, \lambda^c; \Delta, \Psi_0, E] &= \frac{1}{N} \langle \Psi_0 | \hat{H}^{\text{qp}}[R, \lambda] | \Psi_0 \rangle \\ &+ E(1 - \langle \Psi_0 | \Psi_0 \rangle) + \sum_i \left[\langle \Phi_i | \hat{H}_i^{\text{emb}}[D, \lambda^c] | \Phi_i \rangle \right. \\ &+ E_i^c(1 - \langle \Phi_i | \Phi_i \rangle) \left. - \sum_i \left[\sum_{ab} [\lambda_i + \lambda_i^c]_{ab} [\Delta_i]_{ab} \right. \right. \\ &\left. \left. + \sum_{ca\alpha} ([D_i]_{a\alpha} [R_i]_{c\alpha} [\Delta_i(\mathbf{1} - \Delta_i)]_{ca}^{\frac{1}{2}} + \text{c.c.}) \right] \right], \quad (2) \end{aligned}$$

where H_{qp} is the quasiparticle Hamiltonian and H_{emb} is the embedding Hamiltonian, and $|\Psi_0\rangle$ and $|\Phi_i\rangle$ are their wavefunction, respectively. The quasiparticle Hamiltonian is as follows:

$$H^{\text{qp}} = \sum_{\mathbf{k}} \sum_{ab} \left[\sum_{\sigma} R_{a\sigma} \epsilon_{\mathbf{k},\sigma} R_{\sigma b}^{\dagger} + \lambda_{ab} \right] f_{\mathbf{k}a}^{\dagger} f_{\mathbf{k}b}, \quad (3)$$

where $\sigma \in \{\uparrow, \downarrow\}$ is the physical spin degrees of freedom and a, b corresponds to the auxiliary quasiparticle degrees of freedom f_a , whose size can be systematically increased to improve the accuracy of g-RISB. The matrices $[R_i]_{a\sigma} \equiv \sum_b \langle \Phi_i | c_{i\sigma}^{\dagger} c_{ib} | \Phi_i \rangle [\Delta_i(1 - \Delta_i)]_{ba}^{-1/2}$ and

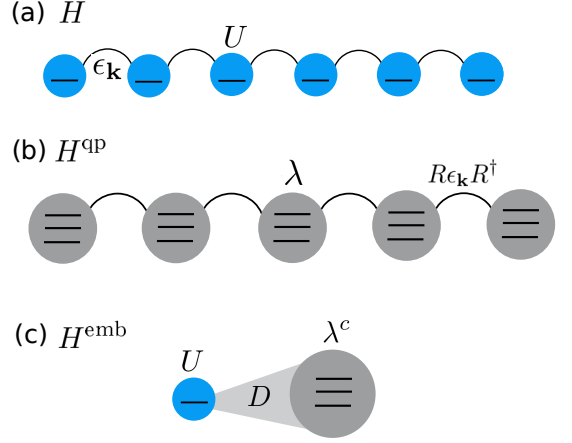


Figure 1. Schematic representation of the (a) original Hubbard model H , (b) non-interacting quasiparticle Hamiltonian H^{qp} , and (c) interacting embedding impurity model H^{emb} . We use three bath sites, including the ghost orbitals, to illustrate the structure.

λ correspond to the quasiparticle renormalization matrix and the renormalized potential, respectively. The Δ_i corresponds to the local quasiparticle density matrix. In this work, we use up to seven auxiliary quasiparticle spin-orbitals, *i.e.*, $a, b \in \{1 \uparrow, 1 \downarrow, \dots, 7 \uparrow, 7 \downarrow\}$. Note that the minimal single quasiparticle-orbital, $a, b \in \{1 \uparrow, 1 \downarrow\}$, recovers the original RISB approach.

The embedding Hamiltonian has the following form:

$$\begin{aligned} \hat{H}_i^{\text{emb}} &= U \hat{n}_{i\uparrow} \hat{n}_{i\downarrow} - \sum_{\sigma} \mu \hat{n}_{i\sigma} \\ &+ \sum_{a\sigma} \left([D_i]_{a\sigma} \hat{c}_{i\sigma}^{\dagger} \hat{f}_{ia} + \text{h.c.} \right) + \sum_{ab} [\lambda_i^c]_{ab} \hat{f}_{ib} \hat{f}_{ia}^{\dagger}, \quad (4) \end{aligned}$$

where D and λ^c describe the hybridization and the bath potential, respectively. The schematic representation of the two Hamiltonian is shown in Fig. 1. Note the g-RISB H_{emb} is similar to the DMFT impurity model with the discretized bath orbitals.

The two Hamiltonians are coupled with each other through the following self-consistent g-RISB equations:

$$\frac{1}{N} \left[\sum_{\mathbf{k}} n_f (R \epsilon_{\mathbf{k}} R^{\dagger} + \lambda) \right]_{ba} = [\Delta_i]_{ab} \quad (5)$$

$$\frac{1}{N} \left[\sum_{\mathbf{k}} \epsilon_{\mathbf{k}} R^{\dagger} n_f (R \epsilon_{\mathbf{k}} R^{\dagger} + \lambda) \right]_{\sigma a} = \sum_{a\sigma} [D]_{c\sigma} [\Delta_i(\mathbf{1} - \Delta_i)]_{ac}^{\frac{1}{2}} \quad (6)$$

$$\sum_{cd\sigma} \frac{\partial}{\partial [\Delta_i]_{ab}} \left([\Delta(\mathbf{1} - \Delta)]_{cd}^{\frac{1}{2}} D_{d\sigma} R_{c\sigma} + \text{c.c.} \right) + [\lambda + \lambda^c]_{ab} = 0 \quad (7)$$

$$H_i^{\text{emb}}|\Phi_i\rangle = E^c|\Phi_i\rangle \quad (8)$$

$$\langle\Phi_i|c_{i,\sigma}^\dagger f_{i,a}|\Phi\rangle - \sum_c [\Delta(\mathbf{1} - \Delta_i)]_{ac}^{\frac{1}{2}} [R_i]_{c\sigma} = 0 \quad (9)$$

$$\langle\Phi_i|f_{ib}f_{ia}^\dagger|\Phi_i\rangle - [\Delta_i]_{ab} = 0 \quad (10)$$

where n_f is the Fermi function, and the variables R , λ , D , λ^c are determined self-consistently. With the converged R and λ , one can compute the Green's function from

$$G_\sigma(\mathbf{k}, \omega) = R_{\sigma a}^\dagger [\omega + i0^+ - R\epsilon_{\mathbf{k}}R^\dagger + \lambda]_{ab}^{-1} R_{b\sigma} \quad (11)$$

and the self-energy can be determined from the Dyson equation

$$\Sigma_\sigma(\omega) = [G_\sigma^0(\mathbf{k}, \omega)]^{-1} - [G_\sigma(\mathbf{k}, \omega)]^{-1}. \quad (12)$$

Note that the self-energy is momentum independent in g-RISB^{21,22}. The quasiparticle renormalization weight is determined from

$$Z_\sigma = \left[1 - \frac{\partial \text{Re}\Sigma_\sigma(\omega)}{\partial \omega}\bigg|_{\omega \rightarrow 0}\right]^{-1}. \quad (13)$$

In this work, we will focus on the paramagnetic solution so the spin index σ will be suppressed.

B. Dynamical mean-field theory

We apply the DMFT-ED algorithm with the discretized bath orbitals to address the convergence of the bath size on the single-orbital Hubbard model^{30,35,39,47,48}. In particular, we use the Lanczos algorithm to solve for the ground state wavefunction and Green's function^{30,33}. For the bath discretization algorithm, we introduce a fictitious inverse temperature $\beta = 200$ to fit the hybridization function on the Matsubara frequency. For $N_b = 1$, we use the weight function $1/i\omega_n$ to obtain better occupancy and fitting³⁹. For $N_b > 1$, we use the uniform weight function. The number of frequency points used for the hybridization function fitting is $N_{\omega_{\text{max}}} = 200$, and the conjugate-gradient method is utilized for the minimization. In our calculations, we found that the hybridization function fitting is essential to obtain reasonable total energy for $N_b \leq 3$. This feature is not reported in the literature, where most studies focus on the spectral function, quasiparticle weight, and the double occupancy^{30,35,39,47,48}.

We also performed DMFT calculations with CTQMC solver⁴⁹, which gives us numerically-exact solutions on the Bethe lattice. The maximum entropy method is utilized for the analytic continuation of Green's functions⁵⁰.

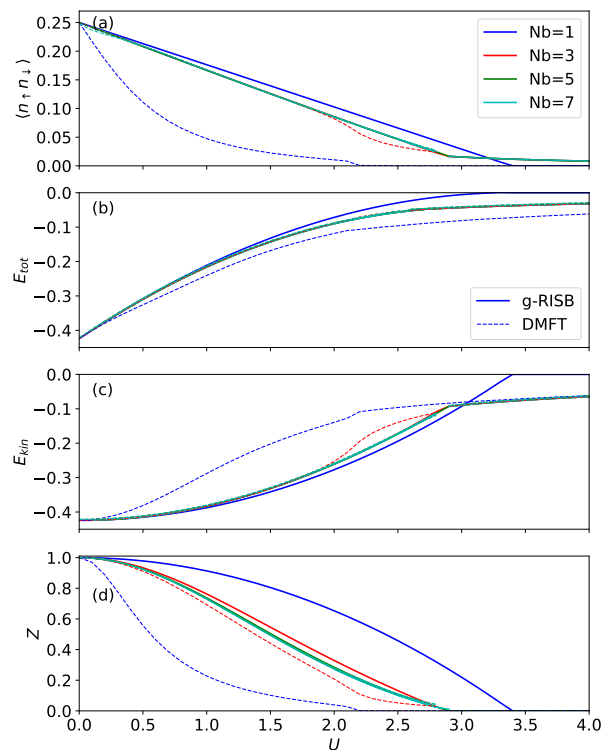


Figure 2. (a) Double occupancy $\langle n_\uparrow n_\downarrow \rangle$, (b) total energy E_{tot} , (c) kinetic energy E_{kin} , and (d) quasiparticle weight Z as a function of coulomb interaction U with increasing bath size N_b at half-filling. The g-RISB and DMFT are shown as solid lines and dashed lines, respectively.

III. RESULTS

A. Half-filled Hubbard model

The double occupancy $\langle n_\uparrow n_\downarrow \rangle$, total energy E_{tot} , kinetic energy E_{kin} , and quasiparticle weight Z as a function of Coulomb interaction U with the increasing numbers of bath orbitals N_b are shown in Fig. 2. Our results indicate that both methods converge with less than 5% error at $N_b = 5$ for all the static physical quantities. For all sizes of the bath, we found that g-RISB generally produces a more accurate double occupancy and total energy closer to the converged value.

Figure 3 provides us with a closer look into the convergence behavior of the double occupancy, total energy, kinetic energy, and the quasiparticle weight at $U = 2.4$ in the metallic phase. Our results show that the g-RISB energy and the double occupancy converge rapidly at $N_b = 3$ with less than 1% error, while DMFT-ED requires $N_b = 5$ to reach the same level of convergence. The quasiparticle weight requires $N_b = 5$ to converge to less than 5% error in both methods. All the observables converge to the DMFT solutions with the CTQMC solver at inverse temperature $\beta = 200$, indicated by the black horizontal line, where the small discrepancy is originated

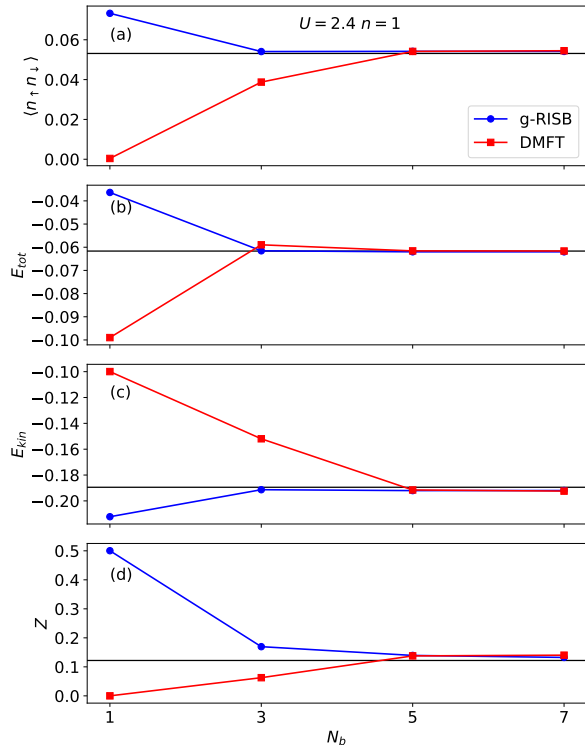


Figure 3. (a) Double-occupancy $\langle n_{\uparrow}n_{\downarrow} \rangle$, (b) total energy E_{tot} , (c) kinetic energy E_{kin} , (d) and quasiparticle weight Z as a function of bath size N_b for $U = 2.4$ at half-filling. The black horizontal line indicates the infinite bath limit with CTQMC solver at inverse temperature $\beta = 200$.

from the finite temperature effect.

The convergence behavior in the insulating phase at $U = 3.5$ is shown in Fig. 4. We found that both methods give reliable energy and double occupancy, and that $N_b = 3$ yields values with errors lower than 1% with respect to the CTQMC value, indicated by the black horizontal line.

We now discuss the g-RISB spectral function with increasing bath size shown in Fig. 5. For $N_b = 1$, corresponding to the standard RISB approach, the spectral function are renormalized following the Brinkman-Rice scenario⁵¹, where the incoherent Hubbard bands are absent. Therefore, the density of states vanishes in the Mott insulating phase where $Z = 0$. On the other hand, with $N_b = 3$, g-RISB can capture reliable Mott insulator solutions where the spectral function shows two incoherent Hubbard bands. The incoherent Hubbard bands also emerge in the metallic spectral functions, and the quasiparticle renormalization is significantly improved, as shown in Fig. 2. For $N_b > 3$, we see the additional bath orbitals introduce more peaks in the spectral functions. The position of the peaks is close to the poles in the DMFT spectral function shown in Fig. 5 with ED and $N_b = 7$. The DMFT spectral functions with CTQMC solver are also shown for comparison.

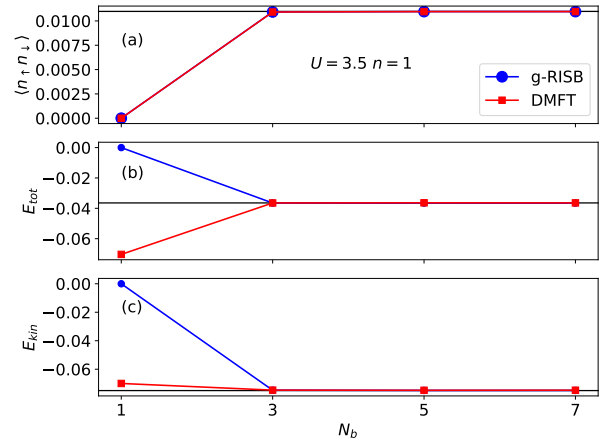


Figure 4. (a) Double occupancy $\langle n_{\uparrow}n_{\downarrow} \rangle$, (b) total energy E_{tot} , and (c) kinetic energy E_{kin} as a function of bath size N_b for $U = 3.5$ at half-filling. The black horizontal line indicates the infinite bath limit with CTQMC solver at inverse temperature $\beta = 200$.

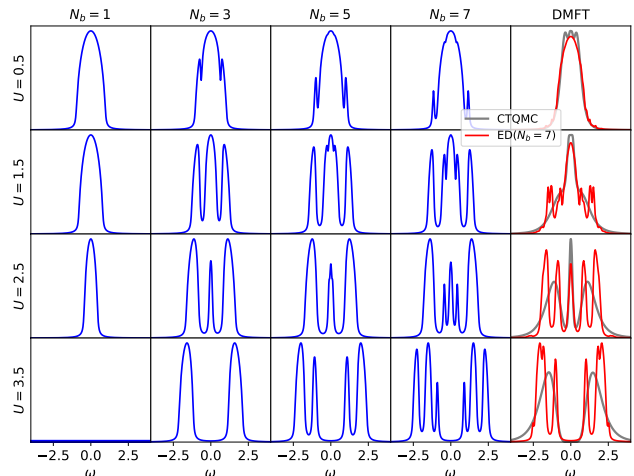


Figure 5. Density of states on Bethe lattice for different values of Coulomb interaction U and bath size N_b (including bath and ghost-orbitals) at half-filling. The right column is the DMFT density of states with ED (bath size $N_b = 7$) and the CTQMC solvers.

B. Doped Hubbard model

The double occupancy, total energy, kinetic energy, and quasiparticle weight of the doped Hubbard model as a function of filling n at $U = 2.4$ are shown in Fig. 6. We found that g-RISB again produces more accurate energies and double occupancy for all electron fillings which are converged at $N_b = 3$ with less than 1% error. On the other hand, DMFT-ED requires $N_b = 5$ to reach the same level of convergence. Both methods converge all physical quantities to less than 5% error at $N_b = 5$.

Figure 7 shows a closer look into the convergence behavior as a function of bath size N_b for $U = 2.4$ and

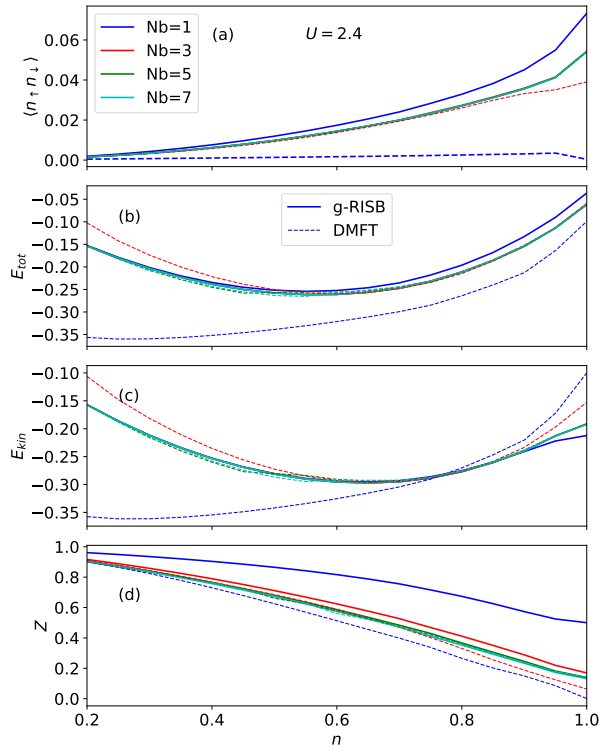


Figure 6. (a) Double occupancy $\langle n_{\uparrow}n_{\downarrow} \rangle$, (b) total energy E_{tot} , kinetic energy E_{kin} , and (d) quasiparticle weight Z as a function of electron filling n with increasing bath size N_b at $U = 2.4$. The g-RISB and DMFT are shown as solid lines and dashed lines, respectively.

filling $n = 0.75$. Our results show again that g-RISB's energy converges rapidly with $N_b = 3$, while DMFT-ED requires $N_b = 5$ to reach the same accuracy. Also, there are small differences between the DMFT-ED energy and the g-RISB energy, where the g-RISB converges to the CTQMC values indicated by the horizontal black line. The discrepancy between the DMFT-ED and the CTQMC results may be attributed to the effect of the artificial temperature introduced in the bath-fitting procedure. On the other hand, the double occupancy and the quasiparticle weight of the two methods both converge to the CTQMC values.

Finally, we report the spectral functions for different fillings and bath sizes in Fig.8. For $N_b = 1$, we again see that g-RISB reduces to the standard RISB approach where the incoherent Hubbard bands are absent, and the band renormalization is of Brinkman-Rice scenario. For $N_b = 3$, g-RISB can capture both the quasiparticle peak and the Hubbard bands, while the higher energy incoherent bands are not captured. For $N_b > 5$, we see the high energy incoherent peaks are included and gradually shifted towards positions in agreement with the spectral function obtained with DMFT-CTQMC (and with DMFT-ED with $N_b = 7$ bath sites).

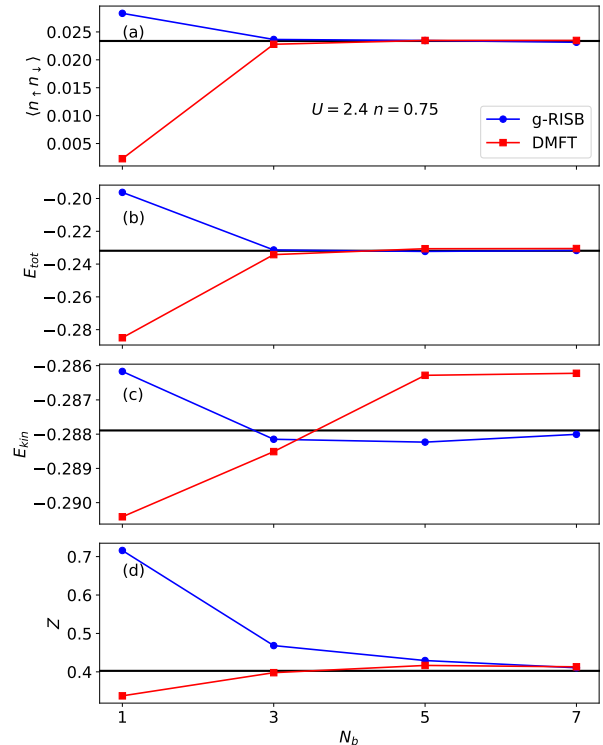


Figure 7. (a) Double-occupancy $\langle n_{\uparrow}n_{\downarrow} \rangle$, (b) total energy E_{tot} , (c) kinetic energy E_{kin} , and (d) quasiparticle weight Z as a function of bath size N_b for $U = 2.4$ at electron filling $n = 0.75$. The black horizontal line indicates the infinite bath limit with CTQMC solver at inverse temperature $\beta = 200$.

n	$N_b = 1$	$N_b = 3$	$N_b = 5$	$N_b = 7$	CTQMC
1	-0.03637	-0.06155	-0.06189	-0.06199	-0.0621±0.0001
0.75	-0.21829	-0.23158	-0.23189	-0.23190	-0.2319±0.0001

Table I. The g-RISB total energy at $U = 2.4$ and filling $n = 1$ and $n = 0.75$ with different numbers of bath orbitals N_b . The DMFT energy at $\beta = 200$ with the CTQMC solver is shown for comparison.

C. Variational property

It is important to note that the g-RISB approach²³ can be also formulated as a variational extension of the Gutzwiller approximation^{21,22}. From this perspective, the total energy is evaluated by computing the expectation value of the Hamiltonian with respect to a variational wavefunction. Therefore, the g-RISB is variational in the limit of infinite coordination, *i.e.*, the g-RISB approximation to the total energy provides us with an upper bound to the exact value. Indeed, this variational behavior is observed numerically in all of our calculations. As an example, we illustrate this in Tab. I) for a few cases, where we see that the total energy converges towards the exact DMFT values from above as a function of the total number of bath sites N_b .

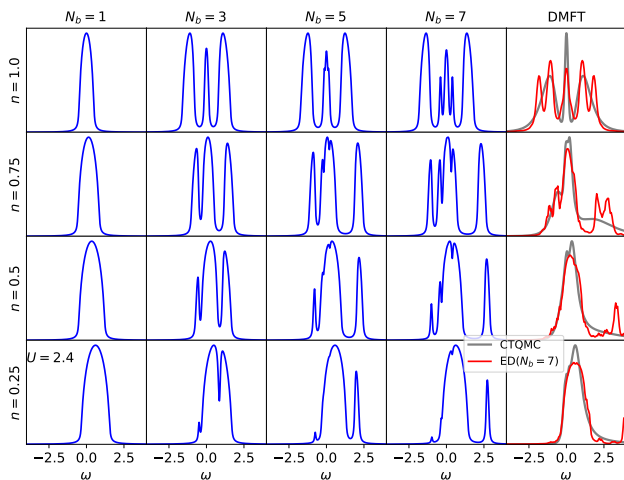


Figure 8. Density of states on Bethe lattice for different electron filling n and bath size N_b (including bath and ghost-orbitals) at $U = 2.4$. The right column is the DMFT density of states with ED (bath size $N_b = 7$) and CTQMC solver.

IV. CONCLUSIONS

We have compared the accuracy of g-RISB and DMFT on the single-band Hubbard model, as a function of the number of bath sites in the embedding impurity Hamiltonian. Our benchmark calculations showed that the accuracy of g-RISB can be systematically improved by increasing the number of bath sites, similar to DMFT. Moreover, we observed that g-RISB is systematically more accurate than DMFT for the ground-state observables with a few bath sites, while the relative accuracy of these methods is generally comparable for the quasiparticle weight and the spectral function. In addition, we observed that g-RISB satisfies the variational principle in infinite dimensions, as the total energy decreases monotonically towards the exact value as a function of the number of bath sites, suggesting that the g-RISB wave-

function may approach the exact ground state in infinite dimensions.

The g-RISB only requires the ground state static density matrix for self-consistency calculations. Therefore, it circumvents the problem of evaluating the excited states (which are necessary for computing the impurity Green's function in DMFT), and opens the possibility of employing efficient ground-state wavefunction-based techniques as impurity solvers.^{41–46,52–61} Our results, which were obtained for a range of interaction strengths and filling factors, indicate that the g-RISB provides us with accurate energies and ground-state properties at small bath sizes, and that it has a relatively low computational cost compared to other methods.

Future research could explore the limitations and potential improvements of the g-RISB theory, and compare it with other quantum embedding approaches for more realistic systems. Overall, our results suggest that g-RISB is a promising method for first principle simulations of strongly correlated matter, which can capture the behavior of both static and dynamical observables with high accuracy, at a relatively low computational cost.

ACKNOWLEDGMENTS

The authors thank Garry Goldstein for the careful reading of the manuscript and the useful comments. T.-H. L and G. K. were supported by the U.S. Department of Energy, Office of Science, Office of Advanced Scientific Computing Research and Office of Basic Energy Sciences, Scientific Discovery through Advanced Computing (SciDAC) program under Award Number DE-SC0022198. NL gratefully acknowledges funding from the Novo Nordisk Foundation through the Exploratory Interdisciplinary Synergy Programme project NNF19OC0057790.

¹ A. Georges, G. Kotliar, W. Krauth, and M. J. Rozenberg, *Rev. Mod. Phys.* **68**, 13 (1996), URL <https://link.aps.org/doi/10.1103/RevModPhys.68.13>.

² G. Kotliar, S. Y. Savrasov, K. Haule, V. S. Oudovenko, O. Parcollet, and C. A. Marianetti, *Rev. Mod. Phys.* **78**, 865 (2006), URL <https://link.aps.org/doi/10.1103/RevModPhys.78.865>.

³ T. A. Maier, M. Jarrell, T. Prushke, and M. Hettler, *Rev. Mod. Phys.* **77**, 1027 (2005), URL <https://link.aps.org/doi/10.1103/RevModPhys.77.1027>.

⁴ G. Knizia and G. K.-L. Chan, *Phys. Rev. Lett.* **109**, 186404 (2012), URL <https://link.aps.org/doi/10.1103/PhysRevLett.109.186404>.

⁵ S. Wouters, C. A. Jimenez-Hoyos, Q. Sun, and G. K.-L. Chan, *Journal of Chemical Theory and Computation* **12**, 2706 (2016), pMID: 27159268,

<https://doi.org/10.1021/acs.jctc.6b00316>, URL <https://doi.org/10.1021/acs.jctc.6b00316>.

⁶ Q. Sun and G. K.-L. Chan, *Accounts of Chemical Research* **49**, 2705 (2016), pMID: 27993005, <https://doi.org/10.1021/acs.accounts.6b00356>, URL <https://doi.org/10.1021/acs.accounts.6b00356>.

⁷ F. Lechermann, A. Georges, G. Kotliar, and O. Parcollet, *Phys. Rev. B* **76**, 155102 (2007), URL <https://link.aps.org/doi/10.1103/PhysRevB.76.155102>.

⁸ N. Lanatà, Y. Yao, C.-Z. Wang, K.-M. Ho, and G. Kotliar, *Phys. Rev. X* **5**, 011008 (2015), URL <https://link.aps.org/doi/10.1103/PhysRevX.5.011008>.

⁹ Potthoff, M., *Eur. Phys. J. B* **32**, 429 (2003), URL <https://doi.org/10.1140/epjb/e2003-00121-8>.

¹⁰ A. A. Kananenka, E. Gull, and D. Zgid, *Phys. Rev. B* **91**, 121111(R) (2015), URL <https://link.aps.org/doi/10.1103/PhysRevB.91.121111>(R)

- 1103/PhysRevB.91.121111.
- 11 D. Zgid and E. Gull, *New Journal of Physics* **19**, 023047 (2017), URL <https://dx.doi.org/10.1088/1367-2630/aa5d34>.
 - 12 I. W. Bulik, G. E. Scuseria, and J. Dukelsky, *Phys. Rev. B* **89**, 035140 (2014), URL <https://link.aps.org/doi/10.1103/PhysRevB.89.035140>.
 - 13 N. Lanatà, Y. Yao, X. Deng, V. Dobrosavljević, and G. Kotliar, *Phys. Rev. Lett.* **118**, 126401 (2017), URL <https://link.aps.org/doi/10.1103/PhysRevLett.118.126401>.
 - 14 T. Ayrál, T.-H. Lee, and G. Kotliar, *Phys. Rev. B* **96**, 235139 (2017), URL <https://link.aps.org/doi/10.1103/PhysRevB.96.235139>.
 - 15 B. Senjean, M. Tsuchiizu, V. Robert, and E. Fromager, *Molecular Physics* **115**, 48 (2017), <https://doi.org/10.1080/00268976.2016.1182224>, URL <https://doi.org/10.1080/00268976.2016.1182224>.
 - 16 J. Bünemann and F. Gebhard, *Phys. Rev. B* **76**, 193104 (2007), URL <https://link.aps.org/doi/10.1103/PhysRevB.76.193104>.
 - 17 N. Lanatà, P. Barone, and M. Fabrizio, *Phys. Rev. B* **78**, 155127 (2008), URL <https://link.aps.org/doi/10.1103/PhysRevB.78.155127>.
 - 18 L. de' Medici, A. Georges, and S. Biermann, *Phys. Rev. B* **72**, 205124 (2005), URL <https://link.aps.org/doi/10.1103/PhysRevB.72.205124>.
 - 19 R. Yu and Q. Si, *Phys. Rev. B* **86**, 085104 (2012), URL <https://link.aps.org/doi/10.1103/PhysRevB.86.085104>.
 - 20 A. B. Georgescu and S. Ismail-Beigi, *Phys. Rev. B* **92**, 235117 (2015), URL <https://link.aps.org/doi/10.1103/PhysRevB.92.235117>.
 - 21 N. Lanatà, T.-H. Lee, Y.-X. Yao, and V. Dobrosavljević, *Phys. Rev. B* **96**, 195126 (2017), URL <https://link.aps.org/doi/10.1103/PhysRevB.96.195126>.
 - 22 M. S. Frank, T.-H. Lee, G. Bhattacharyya, P. K. H. Tsang, V. L. Quito, V. Dobrosavljević, O. Christiansen, and N. Lanatà, *Phys. Rev. B* **104**, L081103 (2021), URL <https://link.aps.org/doi/10.1103/PhysRevB.104.L081103>.
 - 23 N. Lanatà, *Phys. Rev. B* **105**, 045111 (2022), URL <https://link.aps.org/doi/10.1103/PhysRevB.105.045111>.
 - 24 D. Guerci, M. Capone, and M. Fabrizio, *Phys. Rev. Materials* **3**, 054605 (2019), URL <https://link.aps.org/doi/10.1103/PhysRevMaterials.3.054605>.
 - 25 D. Guerci, Ph.D. thesis, International School for Advanced Studies, <https://iris.sissa.it/handle/20.500.11767/103994> (2019).
 - 26 E. Fertitta and G. H. Booth, *Phys. Rev. B* **98**, 235132 (2018), URL <https://link.aps.org/doi/10.1103/PhysRevB.98.235132>.
 - 27 P. V. Sriluckshmy, M. Nusspickel, E. Fertitta, and G. H. Booth, *Phys. Rev. B* **103**, 085131 (2021), URL <https://link.aps.org/doi/10.1103/PhysRevB.103.085131>.
 - 28 Q. Si, M. J. Rozenberg, G. Kotliar, and A. E. Ruckenstein, *Phys. Rev. Lett.* **72**, 2761 (1994), URL <https://link.aps.org/doi/10.1103/PhysRevLett.72.2761>.
 - 29 Y.-H. Zhang and S. Sachdev, *Phys. Rev. Res.* **2**, 023172 (2020), URL <https://link.aps.org/doi/10.1103/PhysRevResearch.2.023172>.
 - 30 M. Caffarel and W. Krauth, *Phys. Rev. Lett.* **72**, 1545 (1994), URL <https://link.aps.org/doi/10.1103/PhysRevLett.72.1545>.
 - 31 M. J. Rozenberg, G. Moeller, and G. Kotliar, *Modern Physics Letters B* **08**, 535 (1994), <https://doi.org/10.1142/S0217984994000571>, URL <https://doi.org/10.1142/S0217984994000571>.
 - 32 A. Liebsch, *Phys. Rev. Lett.* **95**, 116402 (2005), URL <https://link.aps.org/doi/10.1103/PhysRevLett.95.116402>.
 - 33 C. A. Perroni, H. Ishida, and A. Liebsch, *Phys. Rev. B* **75**, 045125 (2007), URL <https://link.aps.org/doi/10.1103/PhysRevB.75.045125>.
 - 34 H. Ishida and A. Liebsch, *Phys. Rev. B* **81**, 054513 (2010), URL <https://link.aps.org/doi/10.1103/PhysRevB.81.054513>.
 - 35 A. Liebsch and H. Ishida, *Journal of Physics: Condensed Matter* **24**, 053201 (2011), URL <https://doi.org/10.1088/0953-8984/24/5/053201>.
 - 36 M. Civelli, M. Capone, S. S. Kancharla, O. Parcollet, and G. Kotliar, *Phys. Rev. Lett.* **95**, 106402 (2005), URL <https://link.aps.org/doi/10.1103/PhysRevLett.95.106402>.
 - 37 B. Kyung, S. S. Kancharla, D. Sénéchal, A. M. S. Tremblay, M. Civelli, and G. Kotliar, *Phys. Rev. B* **73**, 165114 (2006), URL <https://link.aps.org/doi/10.1103/PhysRevB.73.165114>.
 - 38 M. Capone and G. Kotliar, *Phys. Rev. B* **74**, 054513 (2006), URL <https://link.aps.org/doi/10.1103/PhysRevB.74.054513>.
 - 39 M. Capone, L. de' Medici, and A. Georges, *Phys. Rev. B* **76**, 245116 (2007), URL <https://link.aps.org/doi/10.1103/PhysRevB.76.245116>.
 - 40 C. Weber, K. Haule, and G. Kotliar, *Phys. Rev. B* **82**, 125107 (2010), URL <https://link.aps.org/doi/10.1103/PhysRevB.82.125107>.
 - 41 D. Zgid, E. Gull, and G. K.-L. Chan, *Phys. Rev. B* **86**, 165128 (2012), URL <https://link.aps.org/doi/10.1103/PhysRevB.86.165128>.
 - 42 C. Lin and A. A. Demkov, *Phys. Rev. B* **88**, 035123 (2013), URL <https://link.aps.org/doi/10.1103/PhysRevB.88.035123>.
 - 43 Y. Lu, M. Höppner, O. Gunnarsson, and M. W. Haverkort, *Phys. Rev. B* **90**, 085102 (2014), URL <https://link.aps.org/doi/10.1103/PhysRevB.90.085102>.
 - 44 A. Go and A. J. Millis, *Phys. Rev. B* **96**, 085139 (2017), URL <https://link.aps.org/doi/10.1103/PhysRevB.96.085139>.
 - 45 C. Mejuto-Zaera, N. M. Tubman, and K. B. Whaley, *Phys. Rev. B* **100**, 125165 (2019), URL <https://link.aps.org/doi/10.1103/PhysRevB.100.125165>.
 - 46 T. Zhu, C. A. Jiménez-Hoyos, J. McClain, T. C. Berkelbach, and G. K.-L. Chan, *Phys. Rev. B* **100**, 115154 (2019), URL <https://link.aps.org/doi/10.1103/PhysRevB.100.115154>.
 - 47 N.-H. Tong, S.-Q. Shen, and F.-C. Pu, *Phys. Rev. B* **64**, 235109 (2001), URL <https://link.aps.org/doi/10.1103/PhysRevB.64.235109>.
 - 48 H. U. R. Strand, A. Sabashvili, M. Granath, B. Hellsging, and S. Östlund, *Phys. Rev. B* **83**, 205136 (2011), URL <https://link.aps.org/doi/10.1103/PhysRevB.83.205136>.
 - 49 E. Gull, A. J. Millis, A. I. Lichtenstein, A. N. Rubtsov, M. Troyer, and P. Werner, *Rev. Mod. Phys.* **83**, 349 (2011), URL <https://link.aps.org/doi/10.1103/RevModPhys.83.349>.
 - 50 M. Jarrell and J. Gubernatis, *Physics Reports*

- 269**, 133 (1996), ISSN 0370-1573, URL <https://www.sciencedirect.com/science/article/pii/S0370157395000747>.
- ⁵¹ W. F. Brinkman and T. M. Rice, *Phys. Rev. B* **2**, 4302 (1970), URL <https://link.aps.org/doi/10.1103/PhysRevB.2.4302>.
- ⁵² S. R. White, *Phys. Rev. Lett.* **69**, 2863 (1992), URL <https://link.aps.org/doi/10.1103/PhysRevLett.69.2863>.
- ⁵³ S. R. White and R. L. Martin, *The Journal of Chemical Physics* **110**, 4127 (1999), <https://doi.org/10.1063/1.478295>, URL <https://doi.org/10.1063/1.478295>.
- ⁵⁴ G. K.-L. Chan and S. Sharma, *Annual Review of Physical Chemistry* **62**, 465 (2011), pMID: 21219144, <https://doi.org/10.1146/annurev-physchem-032210-103338>, URL <https://doi.org/10.1146/annurev-physchem-032210-103338>.
- ⁵⁵ X. Cao, Y. Lu, P. Hansmann, and M. W. Haverkort, *Phys. Rev. B* **104**, 115119 (2021), URL <https://link.aps.org/doi/10.1103/PhysRevB.104.115119>.
- ⁵⁶ D. Bauernfeind, M. Zingl, R. Triebel, M. Aichhorn, and H. G. Evertz, *Phys. Rev. X* **7**, 031013 (2017), URL <https://link.aps.org/doi/10.1103/PhysRevX.7.031013>.
- ⁵⁷ S. Zhang, J. Carlson, and J. E. Gubernatis, *Phys. Rev. B* **55**, 7464 (1997), URL <https://link.aps.org/doi/10.1103/PhysRevB.55.7464>.
- ⁵⁸ B.-X. Zheng, J. S. Kretchmer, H. Shi, S. Zhang, and G. K.-L. Chan, *Phys. Rev. B* **95**, 045103 (2017), URL <https://link.aps.org/doi/10.1103/PhysRevB.95.045103>.
- ⁵⁹ H. Hao, B. M. Rubenstein, and H. Shi, *Phys. Rev. B* **99**, 235142 (2019), URL <https://link.aps.org/doi/10.1103/PhysRevB.99.235142>.
- ⁶⁰ J. R. Moreno, G. Carleo, A. Georges, and J. Stokes, *Proceedings of the National Academy of Sciences* **119**, e2122059119 (2022), <https://www.pnas.org/doi/pdf/10.1073/pnas.2122059119>, URL <https://www.pnas.org/doi/abs/10.1073/pnas.2122059119>.
- ⁶¹ R. J. Anderson, C. C. J. Scott, and G. H. Booth, *arXiv:2208.07205* (2022), URL <https://arxiv.org/abs/2208.07205>.